

NIST Technical Note 1511

NIST Microwave Power Standards in Waveguide

J. Wayde Allen
Fred R. Clague
Neil T. Larsen
Manly P. Weidman

Radio-Frequency Technology Division
Electronics and Electrical Engineering Laboratory
National Institute of Standards and Technology
325 Broadway
Boulder, Colorado 80303-3328

February 1999



U.S. DEPARTMENT OF COMMERCE, William M. Daley, Secretary
TECHNOLOGY ADMINISTRATION, Gary R. Bachula, Acting Under Secretary for Technology
NATIONAL INSTITUTE OF STANDARDS AND TECHNOLOGY, Raymond G. Kammer, Director

National Institute of Standards and Technology Technical Note
Natl. Inst. Stand. Technol., Tech. Note 1511, 52 pages (February 1999)
CODEN:NTNOEF

U.S. GOVERNMENT PRINTING OFFICE
WASHINGTON: 1999

For sale by the Superintendent of Documents, U.S. Government Printing Office, Washington, DC 20402-9325

CONTENTS

ABSTRACT	1.1
1. INTRODUCTION	1.1
1.1 NIST Microwave Power Standards	1.1
1.2 Bolometer Mount-Microcalorimeter Operation	1.2
2. TRANSFER STANDARD	2.1
2.1 Design	2.1
2.2 Performance	2.2
2.2.1 Effective Efficiency	2.2
2.2.2 Microwave Leakage	2.3
2.2.3 Reflection Coefficient	2.4
3. MICROCALORIMETER	3.1
3.1 Design	3.1
3.2 Thermal Isolation Section	3.1
3.3 Thermopile Assembly	3.3
3.4 Heat Pipe Rings	3.4
3.5 Electronic Control	3.5
3.6 Other Design Features	3.7
4. AUTOMATED CALIBRATION SYSTEM	4.1
4.1 Hardware	4.1
4.2 Software	4.2
5. MEASUREMENT CORRECTION	5.1
5.1 Microcalorimeter Operation Theory	5.1
5.2 Determination of Calorimetric Equivalence Correction Factor g	5.3
6. UNCERTAINTY ANALYSIS	6.1
6.1 Uncertainty in the Correction Factor g	6.1
6.2 Uncertainty Due to Voltage Ratios	6.3
6.2.1 Power Meter Voltage Ratio	6.3
6.2.2 Thermopile Voltage Ratio	6.4
6.2.3 Thermopile and Nanovoltmeter Nonlinearity	6.5
6.3 Other Contributing Factors	6.5
6.4 Random Effects	6.5
6.5 Combined Standard Uncertainty	6.6
6.6 Measurement Assurance	6.6
7. REFERENCES	7.1
APPENDIX 1. Determination of g Using Waveguide Loss Estimates	A1.1
APPENDIX 2. Determination of Incident Power Using a Directional Coupler	A2.1

NIST MICROWAVE POWER STANDARDS IN WAVEGUIDE

J. Wayde Allen, Fred R. Clague, Neil T. Larsen, and Manly P. Weidman

National Institute of Standards and Technology
Boulder, Colorado 80303

The National Institute of Standards and Technology (NIST) microwave power standards in waveguide consist of automated microcalorimeters and associated transfer standards. Each transfer standard is a bolometric dc substitution power detector (a thermistor mount) of special design whose effective efficiency is measured by the microcalorimeter. The general design and operation of the microcalorimeter and transfer standard are described. The theoretical basis for the procedure used to determine the microcalorimeter correction factor, called the calorimetric equivalence, is also described. A detailed uncertainty analysis is included.

Key words: microcalorimeter; microwave; power; standard; waveguide

1. INTRODUCTION

1.1 NIST Microwave Power Standards

The information in this document applies to a series of four power standards built in the same physical configuration except for the waveguide dimensions. The four standards are in the following waveguide bands: WR-42 (18 to 26.5 GHz), WR-22 (33 to 50 GHz), WR-15 (50 to 75 GHz), and WR-10 (75 to 110 GHz). The specific details for the design of each standard plus the results of the uncertainty analysis will be reported in separate documents.

The microwave power standards in use at the National Institute of Standards and Technology (NIST) consist of microcalorimeters and associated transfer standards [1-4]. The microcalorimeter is used to measure a correction for the transfer standard called the effective efficiency. The transfer standard is used to calibrate units submitted by customers. Transfer standards are highly modified commercial bolometric power detectors of the "dc substitution" type, generally called bolometer mounts. Figure 1.1 shows the WR-15 version of the microcalorimeter with the transfer standard attached and figure 1.2 shows it with the transfer standard and heat pipes removed.



Figure 1.1 Microcalorimeter with the transfer standard attached.



Figure 1.2 Microcalorimeter with the transfer standard and heat pipes removed.

1.2 Bolometer Mount-Microcalorimeter Operation

The bolometric power detector uses a heat sensitive resistor (bolometer) which terminates the transmission line and absorbs the microwave energy. Two types of bolometers are used: (1) a platinum wire with a positive temperature coefficient called a "barretter," and (2) a thermistor bead with a negative temperature coefficient. An external power meter supplies a dc current which biases the bolometer to an operating resistance that produces a match with the characteristic impedance of the transmission line. For waveguide mounts, the operating resistance is typically $200\ \Omega$. When microwave energy is applied to the mount, the dc bias supplied by the power meter is automatically reduced to maintain the operating resistance constant [5]. If the microwave energy applied to the mount were totally absorbed by the bolometer element and if the element were heated identically by equal amounts of dc and rf power, then the microwave power would be equal to the dc power reduction. This is called a "substitution type" power meter, because the rf power replaces a portion of the dc bias power. The substituted dc power (also called the bolometric power) is calculated using the equation

$$P_{dc} = \frac{V_1^2 - V_2^2}{R_0}, \quad (1.1)$$

where V_1 is the power meter's output voltage (the dc voltage across the bolometer elements) with no rf, V_2 is the power meter's output voltage with rf, and R_0 is the dc operating resistance of the bolometer element.

The microwave energy incident on a mount is not all absorbed by the bolometer elements. The dielectric and conductor losses in the input connector, the input transmission line, and the bolometer mounting structure, plus any leakage from the mount result in a measurement error characterized by a correction factor called the mount efficiency. This efficiency is always less than 1. In addition, the bolometer elements are not heated identically by equal rf and dc powers. This is known as the rf-dc substitution error. The combination of these two effects, which is measured by the microcalorimeter, is the correction factor defined as the effective efficiency η_e . The rf power absorbed at the input of the mount is calculated by dividing the substituted dc power by the effective efficiency. The mount's effective efficiency is independent of mismatch corrections, which are treated separately at the time of calibration transfer to an unknown mount.

The bolometer elements usually used in the transfer standards are thermistors. Thermistors are rugged and resist burnout in the event of an rf overload. Disadvantages in using thermistors include a continuous drift in the bias current, even in a constant temperature environment. Also, thermistors are not usable in an alternative efficiency measurement technique known as the impedance method [6].

A thermopile is used to determine the steady-state temperature rise of the bolometer mount connected to the microcalorimeter. During the measurement, the microcalorimeter is immersed in a temperature-controlled water bath to minimize the effect of external temperature changes [7, 8]. The measurement procedure determines four parameters at each frequency of interest: the power meter and thermopile output voltages with only dc applied to the mount (V_1 and e_1), and then the same voltages with both rf and dc applied (V_2 and e_2). The effective efficiency η_e is calculated at each test frequency using the equation

$$\eta_e = g \frac{1 - \left(\frac{V_2}{V_1} \right)^2}{\frac{e_2}{e_1} - \left(\frac{V_2}{V_1} \right)^2}. \quad (1.2)$$

The g term in eq (1.2) is a frequency-dependent correction factor for the microcalorimeter-bolometer mount combination. It is also known as the "calorimetric equivalence correction." The uncertainty of the η_e measurement is controlled primarily by the uncertainty in g . The derivation of eq (1.2) and the method of determining g are described in section 5 of this document.

Figure 1.3 shows a typical thermopile output that results when rf is applied to the microcalorimeter and bolometer mount at a single frequency. The change in output from the dc value is about 3 %. A unique software algorithm determines when thermal equilibrium has been attained and the rf can be turned on or off [9].

A typical waveguide transfer standard is calibrated at 1 GHz intervals over the band. Most of the measurement procedure is automated using the system described in section 4. As figure 1.3 shows, even with the automated system the measurement can be very time consuming because of the slow thermal processes involved. In addition, the WR-15 and WR-10 microwave sources at present are manually tuned Gunn diode oscillators rather than a computer-controlled source such as synthesized sweeper. This slows measurements in those bands to about 3 frequencies per day versus 10 or more with a computer-controlled source.

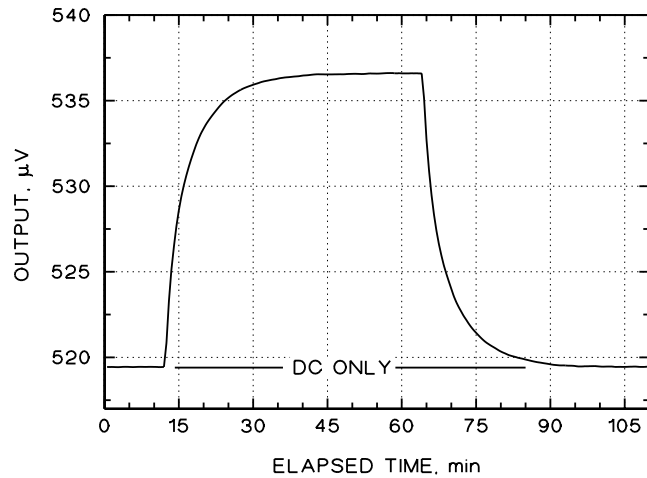


Figure 1.3. Thermopile output of WR-15 microcalorimeter at 75 GHz.

2. TRANSFER STANDARD

2.1 Design

Since the function of the microcalorimeter is to accurately measure the microwave energy dissipated in the mount, there should be minimal thermal resistance between the areas of dissipation and the sensing thermopile. Thus the mount is made primarily of brass and copper and, during the measurement, the thermopile is located very close to the mount. The mount is also gold-plated to prevent deterioration of surface characteristics such as thermal emissivity and electrical conductivity.

The mount will function best as a transfer standard if it has a high effective efficiency. This means that the input transmission line should be made of high electrical conductivity material and have low surface roughness ($\approx 0.5 \mu\text{m}$) so that it will have low rf loss. This is accomplished by using gold-plated electroformed copper for a significant portion of the input transmission line.

Valid measurements of the thermopile output and the power meter voltage cannot be made until the microcalorimeter and mount are in thermal equilibrium with the water bath, a condition indicated by a stable thermopile output. The time to reach stability may be long if the mount has a long thermal time constant because of its mass or internal thermal isolation. An effective way to reduce measurement time is to minimize the thermal mass (heat capacity) of the bolometer mount by reducing its size and eliminating any internal thermal isolation. Unfortunately, the mount design described here did not originally have any thermal isolation, nor has it been possible to reduce its size.

Any rf leakage from the bolometer mount is a first-order source of error in the measurement. The leakage energy, because it is not dissipated in the mount, is not detected by the bolometer element or by the microcalorimeter thermopile. Leakage may radiate or conduct through mechanical joints in the mount body, the dc bias leads, or the rf input connector. The effort to minimize leakage has focused on rf containment by the mount body and rf by-pass of the dc bias circuit.

Also leakage or nonrepeatability at the waveguide flange joint to the microcalorimeter can be a problem. This is addressed by using a flange that eliminates any cocking of the mount when it is attached to the calorimeter [10].

As described earlier, the "substitution type" power meter measures the microwave power in terms of a change in the dc bias power. Any uncertainty in the bolometer's dc resistance will be reflected as an error in the power calculation. Lead-wire and connector contact resistance in the dc bias circuit will generate such an error. The effect of this resistance is eliminated by using a four-wire connection from the bolometer element to a power meter which has external sense leads such as the NIST Type IV power meter (also made commercially). Thus the mount dc bias connector has four conductors, and a four-wire connection is made as close as possible to the thermistor bead.

The physical design features are indicated in figure 2.1, which shows a cross-sectional view of the WR-15 mount with the major parts identified. The thermistor bead assembly is part of a commercial mount. The thermistor interface block with the electroformed copper waveguide section and the cover are custom fabrications. The four-conductor connector is a commercial component.

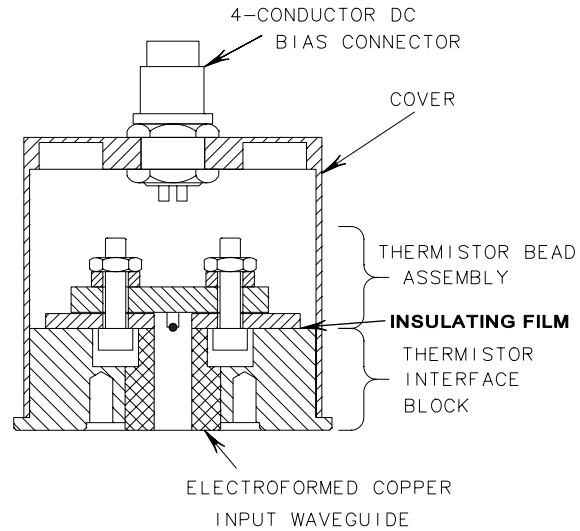


Figure 2.1. Cross section of reference standard.

2.2 Performance

Material presented in this section reports examples of the measured performance of several mounts. Specific results for each standard are reported in the documentation for each waveguide size.

2.2.1 Effective Efficiency

A desirable feature for the mount is that the effective efficiency be a smooth function of frequency. Unfortunately, many thermistor mounts display one or more significant dips in η_e . An example of a very pronounced dip is shown in figure 2.2, which is the calorimeter-measured effective efficiency of a WR-15 mount (WR1503 is a WR-15 mount, serial no. 3). In the dip, η_e changes very rapidly with frequency so the random uncertainty is greater and also interpolation between measured points at or near the dip minimum is not possible.

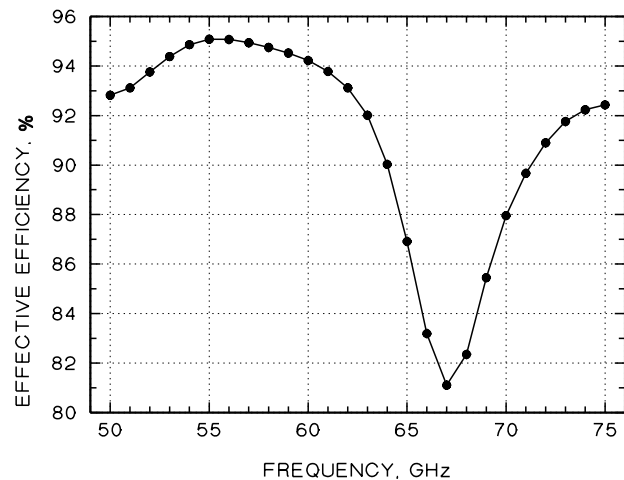


Figure 2.2. Effective efficiency of WR1503.

Not all waveguide mounts exhibit the effect to the degree seen in WR1503. Figure 2.3 shows an example of the more desirable behavior of a WR-10 mount.

As described in the next section, these dips are primarily the result of microwave energy leaking from the mount. A cure that sometimes reduces the leakage and thus minimizes the dip is also described.

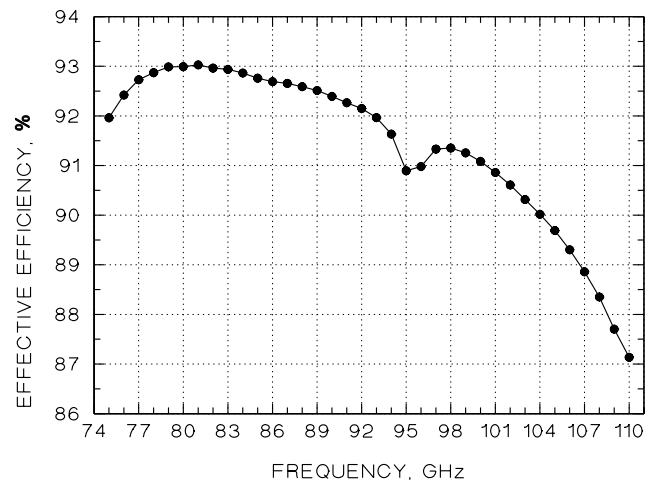


Figure 2.3. Effective efficiency of WR1001.

2.2.2 Microwave Leakage

Detection of microwave leakage from a mount is relatively easy; accurate measurement of its magnitude is not. Development of special techniques and facilities such as the reverberation chamber and the TEM cell make such measurements potentially feasible [11]. Unfortunately, the facilities are not presently available in these waveguide bands, so direct measurement of the leakage has not been possible.

The design objective is to keep the total leakage from the mount at more than 40 dB below the input (less than 0.01 % of the input). Indirect measurements giving approximate values of leakage from mounts in the WR-22 band have been made using a vector network analyzer (VNA). The mount is connected to one port of the VNA, and the leakage is sampled with a waveguide horn connected to the second port. These measurements have shown that the leakage in some portion of the frequency band may be as high as -20 dB, or 1 %, below the input. This leakage could result in a 1 % error in the effective efficiency measurement because it escapes without affecting the thermistor bead or heating the mount (and thus sensed by the microcalorimeter thermopile). The leakage is primarily from the joint in the thermistor bead assembly that contains the insulating film which allows dc bias to be applied to the thermistor bead. See figure 2.1. At frequencies where the leakage is high, the measured effective efficiency shows a pronounced dip as indicated in section 2.2.1.

The dip is caused indirectly by the power-leveling circuit (see section 4.1) which adjusts the microwave source output to maintain an approximate 10 mW of dc-substituted power in the mount. When the leakage increases, the leveler must increase the incident power to the mount to maintain the constant dc-substituted power. This increases the heating from the losses in the mount and results in increased thermopile output and thus an apparent drop in efficiency.

In coaxial mounts the effect has been reduced or eliminated by filling the cavity behind the thermistor bead assembly with a ferromagnetic material (iron powder mixed with two-part RTV;

see [12]). This same material has been applied to the back of a waveguide thermistor assembly (actually, by completely potting the back side) with similar results. At these frequencies (above 18 GHz) the material is probably acting more as a reflector of the leakage than an absorber.

An example of the improvement obtained when this material is used on a WR-22 mount is seen in figure 2.4. In this case the measured leakage with the absorber material dropped to about 40 dB or 0.01 % of the input, which means the leakage error is also less than 0.01 %. Unfortunately, applying the material to the back of a WR-15 mount did not result in the same level of improvement. Thus the material is not the best solution and ultimately the mounts may have to be redesigned.

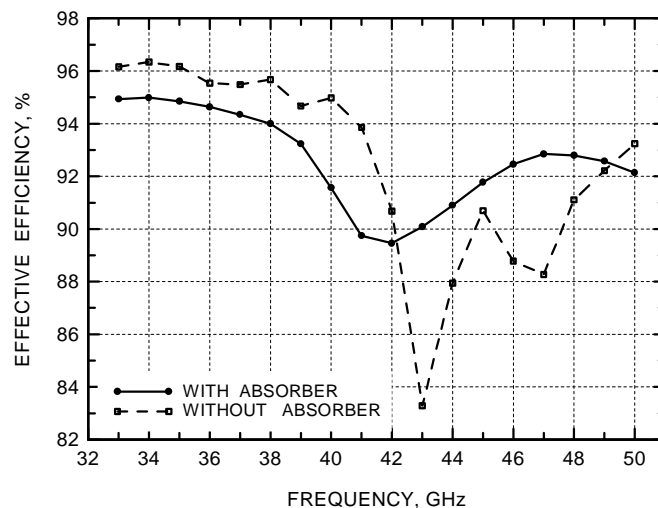


Figure 2.4. Effective efficiency of WR2202.

2.2.3 Reflection Coefficient

An important performance parameter for the transfer standard is the input reflection coefficient. A low reflection coefficient (less than 0.1) is not necessary for the microcalorimeter measurement, but it is desirable for reducing the uncertainty in the calibration transfer and for reducing the minimum output power requirement on the microwave source.

The measurements shown in figure 2.5 were made on a VNA. The values are not less than 0.1, but they agree with typical values for the commercial mount on which the standard is based.

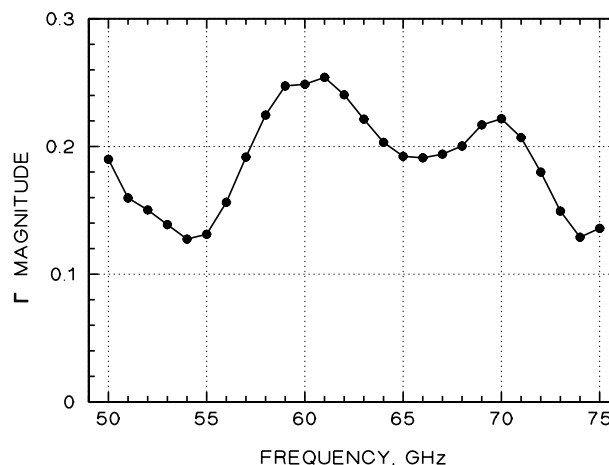


Figure 2.5. Reflection coefficient of WR1503.

3. MICROCALORIMETER

3.1 Design

The microcalorimeter is nonstandard in the sense that it is designed to measure power rather than energy. In other words, this is not a bomb type calorimeter. It does not integrate the total energy input, but rather is designed to measure the rate of energy transfer across a thermal barrier. When power is input, the temperature of the bolometer section rises in proportion to the applied power. This causes heat to flow across the thermal barrier in proportion to the temperature rise. When the heat lost equals the power input, the temperature of the bolometer section stabilizes, and the resulting thermal gradient across the thermopile assembly can be measured. This is similar in concept to the measurement of a dc current by measuring the voltage appearing across a known resistance.

Measurement of the resulting thermal drop does of course require a stable thermal environment. This is achieved by immersing the microcalorimeter in a water bath whose temperature is controlled to nominally $\pm 50 \mu\text{K}$ [7,8]. This effectively isolates the microcalorimeter from temperature fluctuations in the room. However, factors such as water turbulence in the bath itself can cause short-term temperature fluctuations in the microcalorimeter baseplate. These fluctuations are caused by the conversion of the kinetic energy of the moving water to heat upon striking the bottom of the microcalorimeter, and can amount to a few tens of microkelvins. To mitigate this problem, the microcalorimeter is designed so that the actual thermal measurement is not made directly between the bolometer and the microcalorimeter baseplate, but rather between the bolometer mount and an intermediate thermal reference point. This reference point is the outer heat pipe ring mounted on top of the thermal isolation section. Figure 3.1 is a cross sectional view of the base of the microcalorimeter with the reference standard attached. The major parts are labeled to show the relationship between components.

3.2 Thermal Isolation Section

The thermal isolation section is a plastic disk (acrylo-butadiene-styrene, or ABS) that physically separates the bolometer and heat pump ring assemblies from the calorimeter base plate. Details are shown in figure 3.2. The walls of the rf transmission line needed to deliver the rf power to the bolometer mount are formed directly in the plastic base, and the disk is plated with a thin layer of copper and gold. The metallization provides the necessary electrical conductivity while keeping the thermal conductivity as low as possible.

The thermal isolation section is designed to ensure that the thermal paths to the base plate are nearly identical for the bolometer and the outer heat pipe ring. It also increases the thermal resistance which helps slow the response time of the calorimeter to small short-term temperature fluctuations. These balanced thermal paths force any temperature variation in the base plate assembly to affect the bolometer and the reference temperature of the outer heat pump ring identically. Since the temperature rise of the mount is referenced to the outer heat pipe ring, these temperature fluctuations cancel out. This is the well-known "twin Joule" calorimeter design principle described in references [1] and [2].

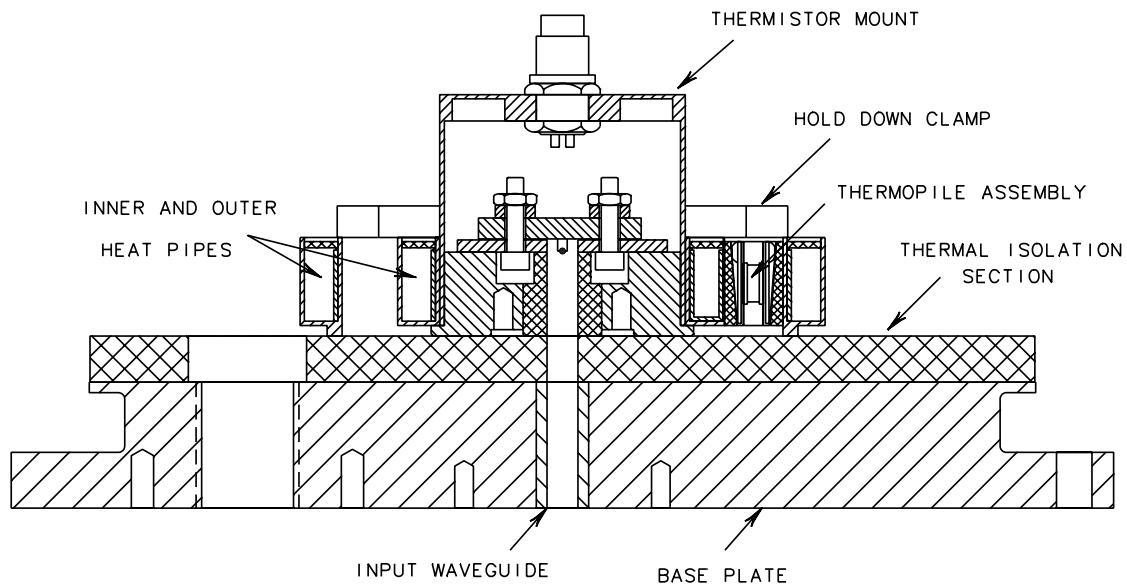


Figure 3.1. Cross section of WR-15 microcalorimeter with an attached mount.

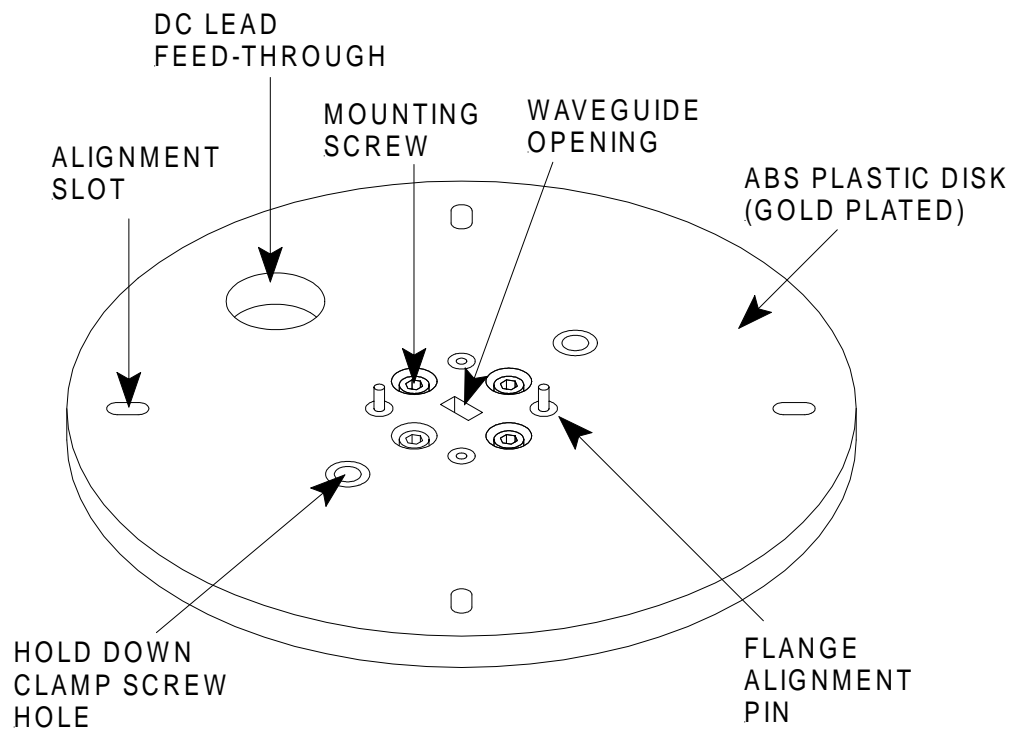


Figure 3.2. Thermal Isolation Section

3.3 Thermopile Assembly

The previous section pointed out that the calorimeter is designed to measure the steady state temperature difference between the bolometric power sensor being tested and the outer heat pipe ring. The thermopile assembly is the structure that provides the primary thermal path between the bolometer and the outer heat pipe ring (thermal reference) and is designed to convert the resulting temperature gradient into a measurable electrical signal. In the older coaxial microcalorimeters the thermopile consisted of a series arrangement of thermocouples made of copper/constantan wire wound around a plastic annulus. In the newer microcalorimeter design this structure has been replaced with a series string of Peltier crystals sandwiched between two platinum resistance thermometers (see figure 3.3) and is about an order of magnitude more sensitive than the old copper/constantan thermopile.

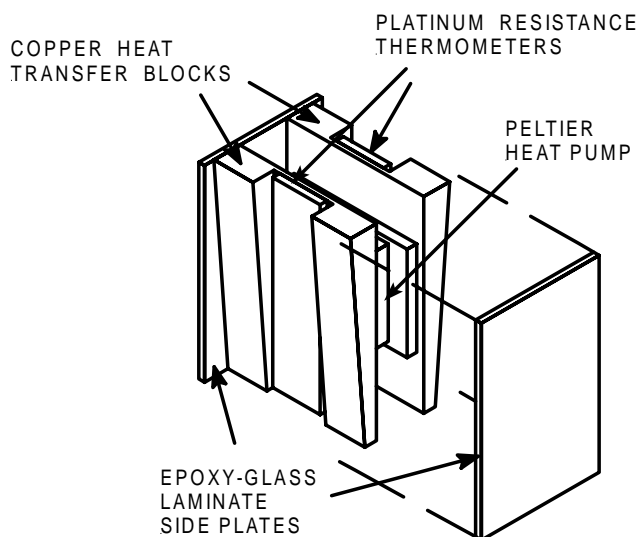


Figure 3.3. Thermopile assembly.

The new thermopile design gives the microcalorimeter two possible modes of operation. First, by measuring the voltage generated by the temperature difference across the Peltier crystal assembly, the microcalorimeter can be used with the same sense-electronics as the older thermocouple-based microcalorimeters, usually nothing more than a sensitive digital voltmeter. For this reason it is not surprising that this has remained the primary operating mode used so far.

In the second, isothermal mode of operation, the platinum resistance thermometers are connected as half of a self-balancing ac bridge circuit. The other half of the bridge circuit consists of an inductive voltage divider. A high gain bandpass amplifier circuit is connected across the center of the bridge and is used to provide current to the Peltier crystals. This circuit will be discussed in more detail in section 3.5. The output signal from the microcalorimeter is provided by monitoring the heat pump bias current.

In this arrangement, the operator initially adjusts the inductive voltage divider to set the starting balance point for the circuit. The bias current to the heat pump assembly is then switched on, so that the heat pump generates a counterflow of heat in direct proportion to the change in the bolometer's heat generation rate. This forces the calorimeter to operate with a constant temperature difference between the bolometer and the outer heat pipe ring. The internal heat generation rate is balanced by the rate of heat transferred to the external water bath. This maintains the thermal energy balance (heat input to heat output) without a corresponding change in the storage of energy in the thermal mass of the calorimeter/bolometer assembly. It also means that the time lag associated with a redistribution of stored energy is ideally eliminated. This should significantly improve the response time of the calorimeter. However, in tests we have made so far, the loss of

precision due to noise in the heat pump feedback control loop has overshadowed the gain in measurement speed. An overall lack of funding and time has prevented us from further pursuing this design option.

3.4 Heat Pipe Rings

As already discussed, the microcalorimeter is designed to measure the temperature difference between the bolometer power sensor being tested, and some reference temperature. The challenge is to design the structure so that the heat generated in the bolometer mount can be easily sampled. Ideally, heat generated at any point in the bolometer should be directed across the thermopile sensor so it can be measured. To this end we designed the calorimeter as a collection of concentric cylinders with the bolometer structure located at the center. This maximizes the contact area with the bolometer. It also minimizes the length of the thermal path from any point on the circumference of the bolometer to the thermopile assembly. Figure 3.4 shows the layout of the structure. Additionally, the thermal masses of the inner bolometer/ring structure and the outer reference ring are designed to be equal so that both structures see the same temperature rise if given the same increase in thermal energy.

In the assembled microcalorimeter, the thermopile assembly serves as a physical spacer and thermal path between the inner ring and the outer thermal reference ring. The thermal isolation section discussed in section 3.2 provides the physical support for the rings themselves. While this means that some heat flows between the rings and the thermal isolation section, as long as the conduction paths from each ring to the thermal isolation section are equal, the relative temperature difference between the two rings remains unaffected.

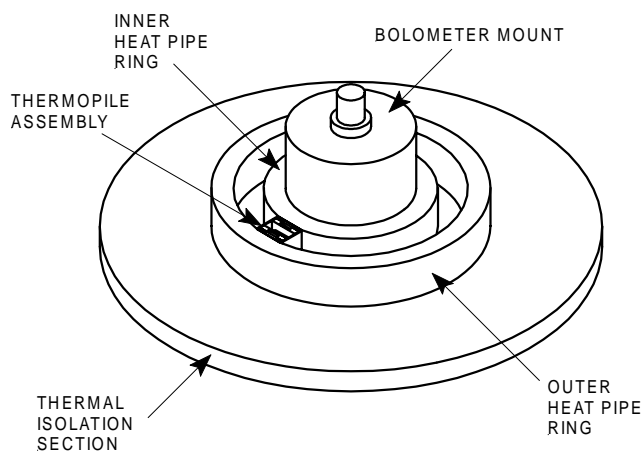


Figure 3.4. Heat pipe rings.

Ideally we would like the thermal conductivity of these rings to have as little effect on the measurement as possible. The purpose of the rings is simply to collect the thermal energy and conduct it to or from the thermopile assembly where the resulting temperature gradient can be measured. Any thermal resistance that these rings offer to the heat flow forms a temperature gradient outside of the thermopile assembly that will not be detected. For this reason, heat pipes which are capable of much higher thermal transfer rates than any known solid materials were chosen for the design.

The heat pipe is basically a closed tube whose walls are lined with a porous copper wick saturated with methanol. The vapor phase fills the remaining open space inside of the structure. Heating any point on this structure vaporizes some of the local methanol resulting in a vapor pressure difference between this region and the coldest section of the tube. This pressure difference drives the vapor

down the tube where it condenses, giving up its latent heat of vaporization to the tube walls. The resulting increase in the liquid phase at the condensation point creates a capillary pressure difference directed towards the heated region. In effect this pumps the liquid back to the vaporization point by capillary action. Figure 3.5 shows a cross sectional view of the heat pipe ring structure. Details concerning the construction of the heat pipe rings are located in the engineering drawings for each individual calorimeter. However a brief overview of the process is presented here.

Construction begins by machining a ring with a U-shaped channel. A stainless steel core is also constructed to fit inside this channel. This stainless steel core is machined to leave space between the walls of the channel in the regions where we wish to place the wick material. This space is filled with copper powder, and the entire assembly is sintered to fuse the powder and adhere it to the walls of the channel. The stainless steel core is then removed, leaving a layer of porous copper wicking material needed for heat pipe action. A lid with a fill tube is then soldered over the top of the channel. Finally, the methanol required to saturate the wicking layer is metered through the fill tube into the heat pipe assembly. The entire assembly is then cooled in liquid nitrogen to lower the vapor pressure of the alcohol and a vacuum pump attached to the fill tube. Once a sufficiently low pressure has been achieved, the fill tube is crimped off, and the structure is allowed to return to room temperature.

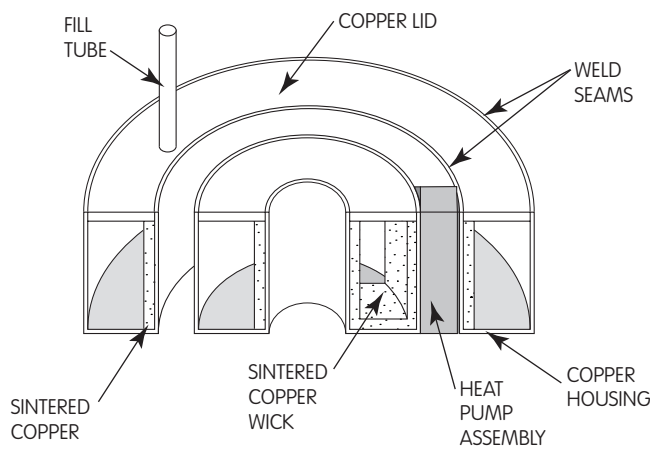


Figure 3.5. Cross sectional view of heat pipe rings (not to scale).

Tests done on these heat pipe rings shortly after their construction showed that the thermal conductivity of the structure exceeded that which could be obtained by making them out of solid copper. However, subsequent testing has given thermal conductivities roughly equal to what one would expect if the rings were simply made of copper. It appears that either the solder seam around the top plate of the structure or the fill tube crimp may have failed allowing air to enter the structure. This may have lowered the overall sensitivity of the calorimeter somewhat, but doesn't affect the measurement accuracy.

3.5 Electronic Control

The instrument requirements needed to run the calorimeter in its traditional thermopile mode are actually quite modest (see figure 4.1). All that is really needed is a voltmeter to read the output from the thermopile assembly. However, the isothermal mode discussed earlier is a bit more complicated.

As was discussed in section 3.3, the thermopile is constructed using two platinum resistance thermometers between which a Peltier heat pump assembly has been sandwiched. These platinum thermometers allow the temperature drop across the thermopile assembly to be directly measured. For the calorimeter to operate in the isothermal mode, the control circuitry monitors the temperature difference between the two platinum thermometers, and forces it to remain constant by adjusting the bias current supplied to the Peltier heat pump crystals. Since we do not really need to know the actual temperature at either of the thermometer points, and since the resistance of the platinum thermometer varies proportionally to its physical temperature, the circuit only needs to establish and maintain a fixed resistance ratio between these two thermometers.

Our prototype sensing circuit is an ac impedance bridge. The platinum resistance thermometers make up half of the bridge circuit with an inductive voltage divider completing the other half (see figure 3.6). Quadrature balance is provided by a differential capacitor connected across the bridge. The bridge design was chosen due to the insensitivity of the inductive voltage divider to temperature

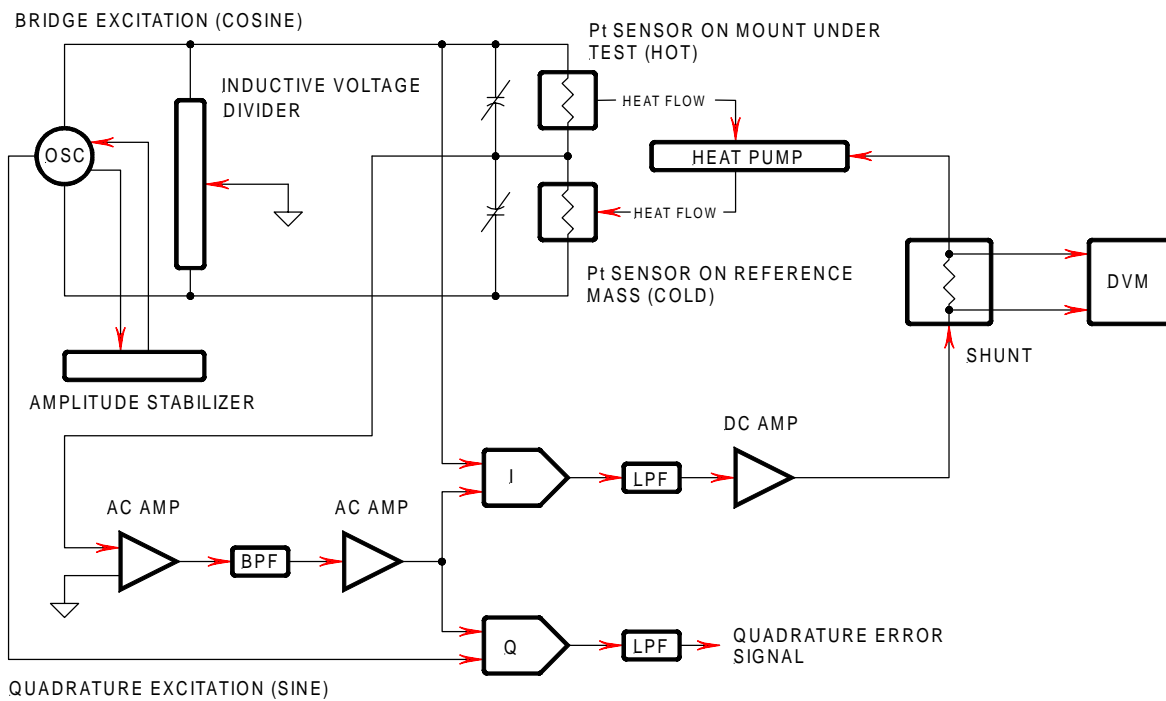


Figure 3.6. Block diagram of the control electronics for isothermal operation.

variation and allows the voltage divider half of the bridge to be physically separated from the calorimeter assembly without introducing balance errors caused by fluctuations of the laboratory room temperature. It also makes the controls for setting the initial bridge balance point accessible outside of the water bath. The balance condition of the bridge circuit is sensed using a low noise lock-in amplifier circuit. The resulting error signal is used to drive the Peltier heat pump crystals in the thermopile assembly to close the loop.

In this mode the calorimeter is placed in the water bath and allowed to stabilize to simplify setting the bridge balance point. With the heat pump current loop open, the bridge circuit is then balanced to establish the reference or set point temperature gradient across the heat pump assembly. The temperature difference between the two thermometers is small; the exact value is unimportant. Once the rough balance has been achieved, the heat pump current loop is closed, actively locking the temperature gradient at this point. When the power dissipated in the thermistor mount changes, due to the introduction of dc or microwave power, the current supplied by the lock-in amplifier changes in such a sense as to maintain the original set point. The current through the heat pump is nearly a linear function of the thermal power passing through it, and it can be measured to provide the data on which the mount efficiency calculation is based. Any small deviations from linearity are easily removed by an empirical fitting function.

As was noted in section 3.3, the reason for considering the isothermal mode is to lower the response time of the calorimeter. If the thermal masses are not allowed to change temperature, due to the feedback of the lock-in control amplifier, then it is not necessary to move energy into or out of the masses (except for an infinitesimal amount). This was expected to provide a significant reduction in the response time of the microcalorimeter. While our initial experiments did show that this technique shortened the measurement time, we ran into problems with noise in the feedback circuitry limiting the precision of the measurement. This problem could ultimately be overcome, but due to lack of project resources, little work is currently being done to refine the technique.

3.6 Other Design Features

The rf input leads, the mount's dc bias leads, and the thermopile's output leads are brought in through the bottom of the microcalorimeter. This provides a more convenient arrangement for removing the top cover and also keeps the leads in the water bath for a greater distance to provide better thermal tempering.

The entire assembly, including the cover, is gold plated for corrosion protection. The gold-plated interior of the cover is polished to provide a high infrared reflectivity. When in use, the unit is suspended in the temperature-controlled water bath by a rod extending from the top of the cover.

4. AUTOMATED CALIBRATION SYSTEM

The automated system allows a completely unattended measurement of the effective efficiency provided the source can be computer controlled. As noted earlier, that is true at present for only WR-42 and WR-22 waveguide bands. The automation is accomplished using mostly off-the-shelf computer-controlled GPIB instrumentation and custom software. The power leveling circuit is an in-house design using the NIST Type II power meter.

4.1 HARDWARE

The system block diagram is shown below in figure 4.1. The actual instrumentation, measurement system console layout and schematic diagram are not shown here because they are essentially identical to the system described in reference [9].

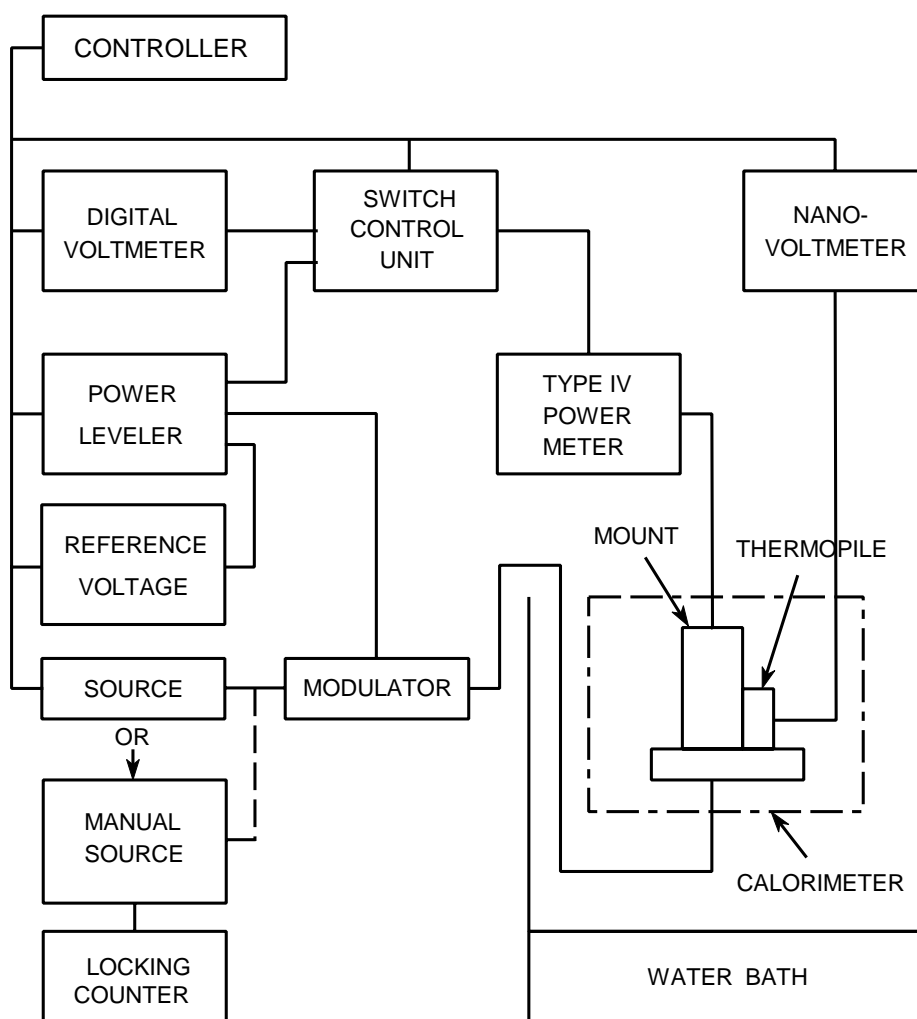


Figure 4.1. Automated calibration system block diagram.

4.2 SOFTWARE

The measurement program is a modification of the software described in reference [9]. That program was written for the Type N coaxial system, but the major features are the same, except that the waveguide version has been written as two programs. The first program controls the measurement and the second provides the post-measurement processing to compute the effective efficiency. In the coaxial version, these two functions are contained in the same program. (A post-measurement computation is required because of the need to correct for the effect of drift in the reference standard bias voltage during the measurement.) Additionally, the waveguide measurement begins without first measuring and comparing data at five test frequencies as is done with the coaxial system.

One of the critical points in the measurement is the determination of when the thermopile output has reached equilibrium or stability. This is especially difficult because the bias voltage for the reference standard essentially never stops changing; in other words, there is continual aging. This means that there is always a drift in the thermopile output, aside from the effect of the microwave loss. In addition, the nanovoltmeter reading of the thermopile output is subject to random fluctuations and noise produced by both the meter and the thermopile itself. The NIST Statistical Engineering Division has developed an algorithm to determine when stability has been reached under these conditions of operation. The algorithm is described in detail in Appendix C of reference [9].

5. MEASUREMENT CORRECTION

The factors listed below all potentially contribute to measurement uncertainty and are included or mentioned in the analysis. In this chapter, a correction is determined for the first three (largest) factors; the remaining are evaluated as uncertainties in section 6.

1. Microcalorimeter microwave transmission line loss.
2. Microcalorimeter/bolometer mount microwave connector loss.
3. Bolometer mount microwave transmission line loss and thermal conductivity effect.
4. Instrumentation errors (voltmeters and dc-substitution power meter).
5. Nonlinearity of thermopile and nanovoltmeter.
6. Bolometer mount microwave leakage.
7. Bolometer mount internal dc lead resistance.
8. Microwave connector repeatability.
9. External temperature stability.

5.1 Microcalorimeter Operation Theory

This section begins with a detailed theoretical development based in part on formulations by both Engen [2] and Weidman [4]. Figure 3.1 is a cross section of the reference standard connected to the calorimeter isolation section and the thermopile. Referring to the figure may be helpful in understanding the following derivation and equations.

The thermopile measures the temperature rise of the attached bolometer mount when the mount is biased with dc alone, or with dc plus rf. The expression for the thermopile output voltage with only dc bias applied to the mount may be written as

$$e_1 = k_1 P_{dc1} = \frac{k_1 V_1^2}{R_0}, \quad (5-1)$$

where k_1 is a proportionality factor characteristic of the thermal transfer path from the mount to the thermopile and is a constant unless the thermopile output is nonlinear. The other terms were originally defined in section 1.2. P_{dc1} is the dc bias power dissipated in the mount, V_1 is the power meter output voltage (equal to the voltage across the bolometer elements) when P_{dc1} is applied, and R_0 is the bolometer element dc operating resistance maintained by the power meter.

With both dc and rf applied to the mount, the new thermopile output voltage is given by

$$e_2 = k_2 (P_{dc2} + aP_b + bP_w + cP_i), \quad (5-2)$$

where k_2 will equal k_1 if the thermopile output is linear, P_{dc2} is the dc bias power dissipated in the mount, P_b is the rf dissipation in and near the bolometer element, P_w is the rf loss in the walls of the mount input section transmission line, P_i is the loss in the isolation section transmission line, and a , b , and c are constants that account for thermal paths that are different than the one described by k_2 .

Equation (5-2) may also be written as

$$e_2 = k_2 \left[P_{dc2} + P_{rf} \left(a \frac{P_b}{P_{rf}} + b \frac{P_w}{P_{rf}} + c \frac{P_i}{P_{rf}} \right) \right], \quad (5-3)$$

where P_{rf} is the total rf power delivered to the mount. Letting

$$q = P_b / P_{rf}, \quad (5-4)$$

$$r = P_w / P_{rf}, \quad (5-5)$$

$$s = P_i / P_{rf}, \quad (5-6)$$

we can write eq (5-3) as

$$e_2 = k_2 [P_{dc2} + P_{rf} (a q + b r + c s)]. \quad (5-7)$$

Then eq (5-7) can be written as

$$e_2 = k_2 (P_{dc2} + g P_{rf}), \quad (5-8)$$

where g is the correction factor given by

$$g = a q + b r + c s. \quad (5-9)$$

g is also called the calorimetric equivalence correction factor because it corrects for the difference in the heating effect of the dc bias versus the rf loss.

Referring back to eqs (5-4) and (5-5), note that

$$q + r = 1 \quad (5-10)$$

because each term represents a fraction of the total rf power absorbed in the mount.

Writing eq (5-8) in terms of V_2 gives

$$e_2 = k_2 \left(\frac{V_2^2}{R_0} + g P_{rf} \right). \quad (5-11)$$

Solving for P_{rf} , we find that

$$P_{rf} = \frac{1}{g} \left(\frac{e_2}{k_2} - \frac{V_2^2}{R_0} \right). \quad (5-12)$$

From eq (5-1), k_1 is given by

$$k_1 = \frac{e_1 R_0}{V_1^2}. \quad (5-13)$$

We also let

$$k_2 \approx k_1, \quad (5-14)$$

which is a good assumption because usually e_1 and e_2 differ by less than 10 %, and tests indicate that at the typical level of e_1 , the thermopile is very linear for these small changes. After substituting eqs (5-13) and (5-14) in (5-12), we have

$$P_{rf} = \frac{1}{g} \left[\left(\frac{e_2}{e_1} \right) \frac{V_1^2}{R_0} - \frac{V_2^2}{R_0} \right] \quad (5-15)$$

or

$$P_{rf} = \frac{1}{g} \left(\frac{V_1^2}{R_0} \right) \left[\left(\frac{e_2}{e_1} \right) - \left(\frac{V_2}{V_1} \right)^2 \right]. \quad (5-16)$$

The definition of effective efficiency (for a bolometric detector) is

$$\eta_e = \frac{P_b}{P_{rf}}, \quad (5-17)$$

where P_b is the bolometric substituted power given by

$$P_b = \frac{1}{R_0} (V_1^2 - V_2^2) = \frac{V_1^2}{R_0} \left[1 - \left(\frac{V_2}{V_1} \right)^2 \right], \quad (5-18)$$

and P_{rf} is the total rf power delivered to the mount. After substituting eqs (5-16) and (5-18) in (5-17), we finally have

$$\eta_e = g \frac{1 - \left(\frac{V_2}{V_1} \right)^2}{\frac{e_2}{e_1} - \left(\frac{V_2}{V_1} \right)^2}. \quad (5-19)$$

5.2 Determination of Calorimetric Equivalence Correction Factor g

This section develops a procedure to determine the correction factor. The process is based on the results of a finite element thermal analysis of the calorimeter and mount plus measurements made with a specially constructed flat short circuit. The short is identical to the transfer standard in physical size and mass and thus identical in thermal characteristics.

Recall that

$$g = a q + b r + c s. \quad (5-9)$$

where a , b , and c are thermal constants.

We look first at the value of the thermal constants. Since a is essentially the thermal path also described by k_1 , we can say by definition that

$$a = 1. \quad (5-20)$$

An approximate value for the thermal constant b has traditionally been obtained by measuring the effect of small heat sources placed in the calorimeter. This process was difficult, not very accurate, and potentially damaging to the calorimeter. A better way to obtain the information is to do a thermal model of the calorimeter using finite element methods. An example, with results of that process for the specific case of the WR-15 calorimeter, is shown in appendix 1. Since all of the calorimeters are identical except for the waveguide size, we assume that the WR-15 results may be applied to all.

Results from the thermal model analysis show that to within 1 %,

$$b \approx 1 . \quad (5-21)$$

By eq (5-10)

$$q = 1 - r , \quad (5-22)$$

and then substituting eqs (5-20, 21, and 22) in (5-9) gives

$$g \approx 1 + c s . \quad (5-23)$$

Thus the only contribution to g comes from the loss in the isolation section.

To determine c we use a flat short. In the same way as eqs (5-1) and (5-2) were developed, the thermopile output with the flat short attached is

$$e_{FS} = k_1 [b P_{FS} + c P_{iFS}] , \quad (5-24)$$

where P_{FS} is the loss in the shorting plate and P_{iFS} is the power dissipated in the calorimeter thermal isolation section. This assumes that the loss in the flat short is not negligible compared to the loss in the isolation section. The constant k_1 continues to be valid because during the flat short measurement it is biased (heated using an external resistor) to produce a level for the e_{FS} measurement that is in the range of e_1 and e_2 .

The loss in the short is just the power dissipated, which is given by

$$P_{FS} = P_{IFS} - P_{RFS} , \quad (5-25)$$

where P_{IFS} is the power incident on the short and P_{RFS} is the power reflected by the short. Since by definition the reflection coefficient of the short is

$$|\Gamma_{FS}|^2 = \frac{P_{RFS}}{P_{IFS}} , \quad (5-26)$$

eq (5-25) can be written as

$$P_{FS} = P_{IFS} (1 - |\Gamma_{FS}|^2) . \quad (5-27)$$

The loss in the thermal isolation section is proportional to the sum of the incident and reflected power passing through it. Since the isolation section is very short, the loss is small. When the flat

short is connected, the isolation section loss is given by

$$P_{iFS} = K_i \left(\frac{P_{IFS}}{1 - K_i} + P_{RFS} \right), \quad (5-28)$$

where K_i is the proportionality factor and, because the loss is small, $K_i \ll 1$. Since K_i is small, eq (5-28) may be written as

$$P_{iFS} \approx K_i (P_{IFS} + P_{RFS}), \quad (5-29)$$

or in terms of the short's reflection coefficient

$$P_{iFS} \approx K_i P_{IFS} (1 + |\Gamma_{FS}|^2). \quad (5-30)$$

Then, substituting eqs (5-21, 27 and 30) in (5-24), we have

$$e_{FS} \approx k_1 P_{IFS} [1 - |\Gamma_{FS}|^2 + c K_i (1 + |\Gamma_{FS}|^2)]. \quad (5-31)$$

Solving for c gives

$$c \approx \frac{e_{FS}}{k_1 K_i P_{IFS} (1 + |\Gamma_{FS}|^2)} - \frac{1 - |\Gamma_{FS}|^2}{K_i (1 + |\Gamma_{FS}|^2)}. \quad (5-32)$$

Next, to determine s recall that

$$s = \frac{P_i}{P_{rf}}, \quad (5-6)$$

where P_i is the power loss in the isolation section with the mount attached and P_{rf} is the net power delivered to the mount.

As with eq (5-30), let

$$P_i \approx K_i P_{IM} (1 + |\Gamma_M|^2), \quad (5-33)$$

where K_i has been defined, P_{IM} is the power incident on the mount, and Γ_M is the mount reflection coefficient. And as with eq (5-27), the net power delivered to the mount is given by

$$P_{rf} = P_{IM} (1 - |\Gamma_M|^2). \quad (5-34)$$

Substituting eqs (5-33 and 34) into (5-6) gives

$$s = K_i \frac{1 + |\Gamma_M|^2}{1 - |\Gamma_M|^2}. \quad (5-35)$$

Finally then, by eqs (5-32) and (5-35)

$$c s \approx \frac{1 + |\Gamma_M|^2}{1 - |\Gamma_M|^2} \left(\frac{e_{FS}}{k_1 P_{IFS} (1 + |\Gamma_{FS}|^2)} - \frac{1 - |\Gamma_{FS}|^2}{1 + |\Gamma_{FS}|^2} \right), \quad (5-36)$$

and, finally, by eq (5-23)

$$g \approx 1 + \frac{1 + |\Gamma_M|^2}{1 - |\Gamma_M|^2} \left(\frac{e_{FS}}{k_1 P_{IFS} (1 + |\Gamma_{FS}|^2)} - \frac{1 - |\Gamma_{FS}|^2}{1 + |\Gamma_{FS}|^2} \right). \quad (5-37)$$

The incident power P_{IFS} is determined using a directional coupler, where in general terms (see appendix 2),

$$P_I = \frac{P_{3L}}{K_C} \frac{1}{|1 - \Gamma_{GE} \Gamma_L|^2}. \quad (5-38)$$

P_I is the incident power for a load with reflection coefficient of Γ_L , P_{3L} is the side arm power with the load attached, and Γ_{GE} is the equivalent generator reflection of the coupler. K_C is a calibration factor for the coupler (including the waveguide to the calorimeter) given by (also derived in appendix 2)

$$K_C = \frac{P_{3S}}{P_S} \frac{\eta_S (1 - |\Gamma_S|^2)}{|1 - \Gamma_{GE} \Gamma_S|^2}, \quad (5-39)$$

where P_{3S} is the coupler side arm power when a standard power meter is attached to the output (arm 2), P_S is the reading of the power standard, η_S is the effective efficiency and Γ_S is the reflection coefficient of the standard. We can then combine eqs (5-38) and (5-39) to give

$$P_I = \frac{P_S}{\eta_S (1 - |\Gamma_S|^2)} \frac{P_{3L}}{P_{3S}} \frac{|1 - \Gamma_{GE} \Gamma_S|^2}{|1 - \Gamma_{GE} \Gamma_L|^2}. \quad (5-40)$$

For P_{IFS} , eq (5-40) becomes

$$P_{IFS} = \frac{P_S}{\eta_S (1 - |\Gamma_S|^2)} \frac{P_{3FS}}{P_{3S}} \frac{|1 - \Gamma_{GE} \Gamma_S|^2}{|1 - \Gamma_{GE} \Gamma_{FS}|^2}. \quad (5-41)$$

If it is not possible to measure the phase of Γ_{GE} , the values of K_C and the incident power can only be bracketed based on worst case phase combinations. Then eq (5-41) becomes,

$$P_{IFS} = \frac{P_S}{\eta_S (1 - |\Gamma_S|^2)} \frac{P_{3FS}}{P_{3S}} \frac{(1 \mp |\Gamma_{GE}| |\Gamma_S|)^2}{(1 \pm |\Gamma_{GE}| |\Gamma_{FS}|)^2}, \quad (5-42)$$

which means that g , calculated using eq (5-37), will also lie between bracketed values.

It is also possible to calculate a value for the correction factor based on theoretical estimates of the waveguide loss. The calculation, which is described in appendix 1, offers a way to independently

check the measured result.

In the derivation of eq (5-37) for g , the effect of the location of the standing wave that is heating the isolation section is not addressed. With the flat short attached, the points of maximum heating are generally not at the same locations as when the mount is connected. If the isolation section were long compared to the guide wavelength the effect of the difference in heating locations would be reduced, but for the microcalorimeters described here the length of the isolation section is comparable to the guide wavelength. To address this situation the measurement with the short is made at the frequency in each band where the loss in the narrow walls is out of phase 180° with the loss in the broad walls [13,14]. Since the heating effect should be fairly well integrated by the calorimeter structure, the effect of the total power loss in the standing wave from the short is uniform with distance along the guide at that frequency. Evidence based on results of the calculation described in appendix 1 and on past evaluations of older waveguide calorimeters indicate that g is not a strong function of frequency. Thus the value determined at this single frequency is used for the whole band.

6. UNCERTAINTY ANALYSIS

From section 5.1, the expression for η_e is

$$\eta_e = g \frac{1 - \left(\frac{V_2}{V_1}\right)^2}{\frac{e_2}{e_1} - \left(\frac{V_2}{V_1}\right)^2}. \quad (5-19)$$

Equation (5-19) can be simplified by letting

$$F_V = \frac{V_2}{V_1} \quad (6-1)$$

and

$$f_e = \frac{e_2}{e_1}, \quad (6-2)$$

so eq (5-19) becomes

$$\eta_e = g \frac{1 - F_V^2}{f_e - F_V^2}. \quad (6-3)$$

With the assumption that the variables g , F_V , and f_e are independent and their uncertainties can be expressed as a standard error, differentiating eq (6-3) and using a sum of squares combination gives

$$\Delta\eta_e^2 = \left(\frac{1 - F_V^2}{f_e - F_V^2}\right)^2 \Delta g^2 + g^2 \left(\frac{2 F_V (f_e - 1)}{(f_e - F_V^2)^2}\right)^2 \Delta F_V^2 + g^2 \left(\frac{1 - F_V^2}{(f_e - F_V^2)^2}\right)^2 \Delta f_e^2, \quad (6-4)$$

or in terms of the relative uncertainties

$$\left(\frac{\Delta\eta_e}{\eta_e}\right)^2 = \left(\frac{\Delta g}{g}\right)^2 + \left(\frac{2 F_V^2 (f_e - 1)}{(1 - F_V^2)(f_e - F_V^2)}\right)^2 \left(\frac{\Delta F_V}{F_V}\right)^2 + \left(\frac{f_e}{f_e - F_V^2}\right)^2 \left(\frac{\Delta f_e}{f_e}\right)^2. \quad (6-5)$$

In the following sections we obtain uncertainty expressions for each of the variables.

6.1 Uncertainty in the Correction Factor g

This analysis is based on the last equation for g (eq 5-37) in section 5.2. We assume that the

thermal models of all the calorimeters will exhibit similar behavior so that the value of the thermal constants will continue to be given by eqs (5-20) and (5-21).

From the preceding chapter, substituting (5-1) and (5-40) in (5-37), we find

$$g \approx 1 + \frac{1 + |\Gamma_M|^2}{1 - |\Gamma_M|^2} \left(\frac{e_{FS} P_{dc1} P_{3S} \eta_s (1 \pm |\Gamma_{GE}| |\Gamma_{FS}|)^2 (1 - |\Gamma_S|^2)}{e_1 P_S P_{3FS} (1 \mp |\Gamma_{GE}| |\Gamma_S|)^2 (1 + |\Gamma_{FS}|^2)} - \frac{1 - |\Gamma_{FS}|^2}{1 + |\Gamma_{FS}|^2} \right). \quad (6-6)$$

Again, assuming that the variables are independent and that their uncertainties can be expressed as a standard error, differentiation and sum-of-squares combination of eq (6-6) give the expression

$$\Delta g^2 = \left(\frac{\partial g}{\partial |\Gamma_M|} \right)^2 |\Delta \Gamma_M|^2 + \left(\frac{\partial g}{\partial P_{dc1}} \right)^2 \Delta P_{dc1}^2 + \left(\frac{\partial g}{\partial P_{3S}} \right)^2 \Delta P_{3S}^2 + \dots \quad (6-7)$$

for the uncertainty in g due to uncertainties in each contributing factor (total of 12 variables). Before deriving the expressions for the partial derivatives, we can simplify eq (6-6) by letting

$$M = \frac{1 + |\Gamma_M|^2}{1 - |\Gamma_M|^2} \quad (6-8)$$

and

$$F = \frac{1 - |\Gamma_{FS}|^2}{1 + |\Gamma_{FS}|^2} \quad (6-9)$$

Then

$$g \approx 1 + M \left(\frac{e_{FS} P_{dc1} P_{3S} \eta_s (1 \pm |\Gamma_{GE}| |\Gamma_{FS}|)^2 (1 - |\Gamma_S|^2)}{e_1 P_S P_{3FS} (1 \mp |\Gamma_{GE}| |\Gamma_S|)^2 (1 + |\Gamma_{FS}|^2)} - F \right). \quad (6-10)$$

For the quantities e_{FS} , P_{dc1} , P_{3S} , and η_s , a general expression for the partial derivatives is

$$\frac{\partial g}{\partial x} = \frac{G}{x}, \quad (6-11)$$

where each quantity can be substituted for x . G is given by

$$G = g - 1 + M F. \quad (6-12)$$

For the quantities e_1 , P_S , and P_{3FS} , a general expression for the partial derivatives is

$$\frac{\partial g}{\partial y} = -\frac{G}{y}, \quad (6-13)$$

where each quantity can be substituted for y .

The other partial derivatives are

$$\frac{\partial g}{\partial |\Gamma_M|} = 4 (g - 1) \frac{|\Gamma_M|}{1 - |\Gamma_M|^4} \quad (6-14)$$

$$\frac{\partial g}{\partial |\Gamma_{GE}|} = \frac{\pm 2 G (|\Gamma_{FS}| + |\Gamma_S|)}{(1 \pm |\Gamma_{GE}| |\Gamma_{FS}|) (1 \mp |\Gamma_{GE}| |\Gamma_S|)} \quad (6-15)$$

$$\frac{\partial g}{\partial |\Gamma_S|} = \frac{\pm 2 G (|\Gamma_S| \mp |\Gamma_{GE}|)}{(1 \mp |\Gamma_{GE}| |\Gamma_S|) (1 - |\Gamma_S|^2)} \quad (6-16)$$

$$\frac{\partial g}{\partial |\Gamma_{FS}|} = - \frac{2 G (|\Gamma_{FS}| \mp |\Gamma_{GE}|)}{(1 \pm |\Gamma_{GE}| |\Gamma_{FS}|) (1 + |\Gamma_{FS}|^2)} + \frac{4 M |\Gamma_{FS}|}{(1 + |\Gamma_{FS}|^2)^2}. \quad (6-17)$$

In each of these equations, g also has a double value as indicated and calculated by (6-6).

In the expression for g , as given by eq (6-6), the quantities e_{FS} and e_1 appear as a ratio. In their measurement a correction for the zero offset is made. In terms of the measured quantities these are given by

$$e_{FS} = (e_{FS})_1 - (e_{FS})_0 \quad (6-18)$$

and

$$e_1 = (e_1)_1 - (e_1)_0, \quad (6-19)$$

where the external subscript $_0$ denotes the zero correction value and the external subscript $_1$ denotes the measured value. These terms appear in eq (6-6) as a ratio. As will be explained in the next section, under these circumstances, at least to first order, only the random part of the nanovoltmeter error contributes to the uncertainty.

6.2 Uncertainty Due to Voltage Ratios

6.2.1 Power Meter Voltage Ratio

Differentiating eq (6-1), we obtain the relative uncertainty in F_V

$$\left(\frac{\Delta F_V}{F_V} \right)^2 = \left(\frac{\Delta V_1}{V_1} \right)^2 + \left(\frac{\Delta V_2}{V_2} \right)^2. \quad (6-20)$$

Because of mount drift, V_1 does not remain constant during the measurement, so V_1 is actually an

interpolated value between two end point measurements. V_1 is given by

$$V_1 = V_{1i} + \gamma (V_{1f} - V_{1i}) = (1 - \gamma) V_{1i} + \gamma (V_{1f}), \quad (6-21)$$

where V_{1i} and V_{1f} are the initial and final values of the V_1 measurements and γ is a fraction between 0 and 1. The worst case uncertainty in V_1 is

$$|\Delta V_1| = (1 - \gamma) |\Delta V_{1i}| + \gamma |\Delta V_{1f}|. \quad (6-22)$$

Since both the initial and final values differ by only a small amount and are measured on the same range, a good approximation is $|\Delta V_{1i}| \approx |\Delta V_{1f}|$. Then by eq (6-22), $|\Delta V_1| \approx |\Delta V_{1i}|$, so the uncertainty in V_1 will be no worse (and could be less) than for a single measurement.

A numerical calculation of the uncertainty in η_e due to ΔF_v , which is a function of η_e and P_{rf} , can be made using eqs (6-5) and (6-20).

6.2.2 Thermopile Voltage Ratio

The expression for f_e is given by eq (6-2). In measuring f_e , a correction for the zero offset must be made. This involves measuring e_0 before measuring the dc bias term e_1 or the dc-plus-rf term e_2 . When we take e_0 into consideration, eq (6-2) becomes

$$f_e = \frac{e_2 - e_0}{e_1 - e_0}. \quad (6-23)$$

The uncertainty in f_e is given by

$$\Delta f_e^2 = \left(\frac{e_2 - e_1}{(e_1 - e_0)^2} \right)^2 \Delta e_0^2 + \left(\frac{e_2 - e_0}{(e_1 - e_0)^2} \right)^2 \Delta e_1^2 + \left(\frac{1}{e_1 - e_0} \right)^2 \Delta e_2^2, \quad (6-24)$$

or in terms of the relative uncertainties

$$\left(\frac{\Delta f_e}{f_e} \right)^2 = \left(\frac{e_0 (e_2 - e_1)}{(e_1 - e_0)(e_2 - e_0)} \right)^2 \left(\frac{\Delta e_0}{e_0} \right)^2 + \left(\frac{e_1}{e_1 - e_0} \right)^2 \left(\frac{\Delta e_1}{e_1} \right)^2 + \left(\frac{e_2}{e_2 - e_0} \right)^2 \left(\frac{\Delta e_2}{e_2} \right)^2. \quad (6-25)$$

Like V_1 , e_1 is obtained by linear interpolation, so the uncertainty Δe_1 is also approximately that of a single measurement.

The error in a voltmeter reading is generally specified as a percent of reading factor (α) plus a percent of full scale (β). The factor α comes from the error of the internal reference, while the factor β is due to random and zero correction errors and nonlinearity. In a ratio measurement, if the two voltages are measured on the same scale and close in value, the alpha factor can be neglected. In addition, if the zero drift is explicitly corrected (as in the f_e case), the only contribution to the uncertainty is from the random part of β .

The numerical calculation of the uncertainty in η_e due to Δf_e is based on the applicable parts of eqs (6-5) and (6-25).

An additional factor that may add to Δf_e is the uncertainty in knowing when the thermopile has reached equilibrium. This is a critical element in the measurement. A software algorithm determines when equilibrium has been reached at each measurement frequency. The algorithm is described in appendix C of [9]. It has been tested by letting the measurement continue for several minutes beyond the point the algorithm indicates stability has been reached and noting that the result essentially does not change. While it has not been possible to detect any systematic uncertainty in the process, there is a random component that is included in the uncertainty.

6.2.3 Thermopile and Nanovoltmeter Nonlinearity

The linearity of the thermopile and nanovoltmeter affects the validity of eq (5-14) and thus the ratio f_e . Linearity can be tested by performing a series of measurements on the calorimeter using a mount with a resistor in place of the thermistor bead. A dc bias is applied to the resistor, and the output as measured by the nanovoltmeter is noted as a function of the dc bias power. In other words we look for the expression

$$k = \frac{e}{P_{dc}}, \quad (6-26)$$

to remain constant as P_{dc} is varied between values that give nanovoltmeter outputs e that are approximately equal to e_1 and e_2 . As noted in section 5.1, tests have shown any change to be very small. So rather than develop a correction, we will add any measured deviation to Δf_e .

6.3 Other Contributing Factors

Other factors contributing to the uncertainty are microwave leakage from the mount, resistance in the dc bolometer leads not corrected by the four-wire connection, and Type IV power meter errors. The expressions for these effects, which are developed in sections 6.5 through 6.7 of reference [9], are also applicable to this case and will not be repeated here.

6.4 Random Effects

Uncertainty factors that primarily affect the result randomly are the water bath stability and waveguide flange (the waveguide connector) repeatability. The effect of these will be included in the Type A evaluation of the standard uncertainty for the measurement process.

The Type A evaluation is generally based on repeated measurements of a single reference standard which will continue to be used as a check standard. Ideally, the standard uncertainty for the bolometer mounts should be determined through repeat measurements for each individual mount.

This is impractical due to the time required for a complete set of measurements. Therefore, we assume that the standard uncertainty inherent in all mounts behaves in basically the same fashion, so the standard uncertainty we derive for the check standard mount will apply to the population of mounts as well. Since the observed standard deviations may be different for each frequency, a single value of standard uncertainty which is valid for all frequencies will be based on a "worst case" standard deviation.

6.5 Combined Standard Uncertainty

Table 6.1 is a summary of the how the different uncertainty components will be evaluated. The distribution used to obtain the standard uncertainty and the basis for the analysis is also given. The section in this chapter or in reference [9] that describes the uncertainty is also listed in the table. Definitions of the terms "evaluation type," "distribution," and "standard uncertainty" are found in reference [15].

The largest contributor to the uncertainty is $\Delta|\Gamma_{FS}|$. In fact the combined effect of all the other factors is an order of magnitude smaller.

6.6 Measurement Assurance

One of the most important aspects of maintaining a microcalorimeter system is measurement assurance. Since individual mounts cannot be measured repeatedly, it becomes even more important to ensure that the system is behaving as it should. Several techniques are employed to monitor the system and assure measurement quality. These are described in detail for the coaxial microcalorimeter in reference [9], but they are also used for the waveguide systems. They are basically a set of charts that monitor system behavior through regular measurements made on check standards.

Table 6.1. Uncertainty components.

Uncertainty factor	Section reference	Evaluation type	Distribution	Based on:
Δe_{OS}	6.1	B	Rectangular	Nanovoltmeter measurement
Δp_{dc1}	6.1	B	Rectangular	Voltmeter and Type IV power meter
ΔP_{3S}	6.1	B	Rectangular	Voltmeter and Type IV power meter
$\Delta \eta_s$	6.1	B	Rectangular	Uncorrected calorimeter measurement
Δe_1	6.1	B	Rectangular	Random error in nanovoltmeter meas.
ΔP_s	6.1	B	Rectangular	Voltmeter and Type IV power meter
ΔP_{3OS}	6.1	B	Rectangular	Voltmeter and Type IV power meter
$\Delta \Gamma_M $	6.1	B	Rectangular	Network analyzer measurement
$\Delta \Gamma_{GE} $	6.1	B	Rectangular	Network analyzer measurement
$\Delta \Gamma_S $	6.1	B	Rectangular	Network analyzer measurement
$\Delta \Gamma_{FS} $	6.1	B	Rectangular	Network analyzer measurement
ΔF_V	6.2.1	B	Rectangular	Voltmeter and Type IV power meter
Δf_e	6.2.2	A	Normal	Random part of nanovoltmeter meas. plus end-point determination
Linearity	6.2.3	B	Rectangular	Voltmeters
Mount leakage	2.2.2	B	Rectangular	Indirect measurement
Lead resistance	Ref [9]	B	Rectangular	Not a factor in η_e measurement
Type IV power meter	Ref [9]	B	Rectangular	Op amp offset, reference resistor
Random effects	6.4	A	Normal	Repeated transfer standard meas.

7. REFERENCES

- [1] MacPherson, A.C.; Kerns, D.M. A microwave microcalorimeter. *Rev. Sci. Instrum.* 26(1): 27-33; 1955 January.
- [2] Engen, G.F. A refined x-band microwave microcalorimeter. *J. Res. Nat. Bur. Stand. (U.S.)* 63C(1): 77-82; 1959 July-September.
- [3] Harvey, M.E. WR 15 microwave calorimeter and bolometer unit. *Nat. Bur. Stand. (U.S.) Tech. Note* 618; 1972 May. 33 p.
- [4] Weidman, M.P.; Hudson, P.A. WR 10 millimeter wave microcalorimeter. *Nat. Bur. Stand. (U.S.) Tech. Note* 1044; 1981 June. 11 p.
- [5] Larsen, N.T. A new self-balancing dc-substitution rf power meter. *IEEE Trans. Instrum. Meas.* IM-25: 343-347; 1976 December.
- [6] Engen, G.F. A bolometer mount efficiency measurement technique. *J. Res. Nat. Bur. Stand. (U.S.)* 65C(2): 113-124; 1961 April-June.
- [7] Larsen, N.T. 50 microdegree temperature controller. *Rev. Sci. Instrum.* 39(1): 1-12; 1968 January.
- [8] Harvey, M.E. Precision temperature-controlled water bath. *Rev. Sci. Instrum.* 39(1): 13-18; 1968 January.
- [9] Clague, F.R. A calibration service for coaxial reference standards for microwave power. *Natl. Inst. Stand. Technol. Tech. Note* 1374; 1995 May. 109 p.
- [10] Maury, M.A.; Simpson, G.R. Improved millimeter waveguide flanges improve components and measurements. *Microwave J.* 29(5): 337-346; 1986 May.
- [11] Crawford, M.L.; Koepke, G.H. Design, evaluation, and use of a reverberation chamber for performing electromagnetic susceptibility/vulnerability measurements. *Nat. Bur. Stand. (U.S.) Tech. Note* 1092; 1986 April. 146 p.
- [12] Clague, F.R.; Voris, P.G. Coaxial reference standards for microwave power. *Natl. Inst. Stand. Technol. Tech. Note* 1357; 1993 April. 46 p.
- [13] Brady, M.M. In-line waveguide calorimeter for high-power measurement. *IRE Trans. Microwave Theory Tech.* MTT-10: 359-356; 1962 September.
- [14] Brady, M.M. Correction to "In-line waveguide calorimeter for high-power measurement" - accounting for transverse waveguide wall currents. *IEEE Trans. Microwave Theory Tech.* MTT-11: 152; 1963 March.
- [15] Taylor, B.N.; Kuyatt, C.E. Guidelines for evaluating and expressing the uncertainty of NIST measurement results. *Natl. Inst. Stand. Technol. Tech. Note* 1297 (1994 edition); 1994 September. 20 p.
- [16] Ramo, Simon; Whinnery, John R., *Fields and Waves in Modern Radio*, Second Edition, John Wiley and Sons, New York, NY, 1962.
- [17] Beatty, R.W. Application of waveguide and circuit theory to the development of accurate microwave measurements and standards. *Nat. Bur. Stand. (U.S.) Monograph* 137; 1973 August.
- [18] Yates, B.C.; Counas, G.J. Summary of WR15 Flange Evaluation at 60 GHz. *Nat. Bur. Stand. (U.S.) Tech. Note* 642; 1973 October.
- [19] Fantom, A. *Radio Frequency and Microwave Power Measurement*, IEE Electrical Measurement Series 7, Peter Peregrinus Ltd., 1990.

APPENDIX 1. Determination of g Using Waveguide Loss Estimates

The correction factor g can also be calculated by using the methods in [4]. This includes an estimate of the loss in the microcalorimeter isolation section, the waveguide flange joint, the mount walls, and the shorting plate at the back of the mount.

Again, the basic equation is

$$g = a q + b r + c s + d t, \quad (\text{A1-1})$$

where terms a , b , c , and d represent the relative heating effectiveness at the thermistor bead, the mount walls, the mount waveguide flange and the thermal isolation section, respectively. The quantities q , r , s , and t are power dissipations at the corresponding locations relative to the net power in the mount. Equation (A1-1) explicitly includes the waveguide flange loss as s and the isolation section loss as t , but in eq (5-9) of section 5, both losses are lumped together as s . The heating effectiveness a is the reference for the other three terms, and by definition is unity. The next equation is

$$q = 1 - r - s, \quad (\text{A1-2})$$

which describes the fractional power dissipated in the mount away from the thermistor bead (the walls, the back plate, and the flange). The mount wall and back plate dissipation is combined in r . The isolation section loss t is missing from eq (A1-2) because the effect of the loss there is measured by the microcalorimeter temperature sensor as if it were part of the η_e although it is not. The loss t is corrected for directly rather than proportional to its fractional difference from 1. The loss calculations are used to determine the quantities r , s , and t , which are the fractional part of the power in the incident wave dissipated in different parts of the microcalorimeter and the thermistor mount whose η_e is being measured by the microcalorimeter.

We begin by calculating the waveguide conductor loss α using an equation,

$$\alpha = \frac{R_s}{\eta h} \frac{1 + \frac{2h}{w} (f_c/f)^2}{\sqrt{1 - (f_c/f)^2}}, \quad (\text{A1-3})$$

from Ramo and Whinnery [16], where w and h are the waveguide width and height, η is the characteristic impedance of the dielectric (approximately 377Ω for air), R_s is the surface resistivity of the waveguide conductor, f is the frequency of interest, and f_c is the cutoff frequency of the waveguide. The f_c is $v/2w$ where the length units in v (the velocity of light in air) and w are the same. The conductivity for the gold plated waveguide is used for these calculations with a 20 % increase in loss for surface finish and conductor uncertainty. The conductor uncertainty exists because of the uncertainty in the plating process and was determined experimentally. For all the rectangular waveguides $2h/w$ is 1. The R_s used for the calculations is

$$R_s = 3 \times 10^{-7} \sqrt{f}, \quad (\text{A1-4})$$

where R_s is in ohms and f is the frequency in hertz. The value of 3 in eq (A1-4) is a compromise among the resistivity values published in various references for gold.

The loss per unit length (dB/cm) for the different waveguides at the desired frequency can be calculated using the previous assumptions. With this information we can then determine the contribution to r that is due to loss in the mount walls. The length of the side walls is determined, and after converting from decibels to power ratio, the fractional values for the wall loss can also be calculated.

The loss in the back plate of the mount is calculated using eq (A1-5) which comes from Beatty [17] (eq 5.33, p. 133 should be $4/[\sigma\delta Z_h]$).

$$\frac{P_{SP}}{P_I} = \frac{4}{\sigma \delta Z_h}, \quad (\text{A1-5})$$

where P_I is the incident power, σ is the conductivity of the back plate metal, δ is the skin depth and Z_h is the wave impedance of the waveguide, given by

$$Z_h = \eta \frac{\lambda}{\lambda_g}. \quad (\text{A1-6})$$

The guide wavelength λ_g is

$$\lambda_g = \frac{\lambda}{\sqrt{1 - (f_c/f)^2}}, \quad (\text{A1-7})$$

where λ is the air wavelength. The power reaching the end plate will be less than the power incident at the mount input since much of it will be absorbed by the thermistor bead. But since this factor is such a small part of the overall g calculation, we will assume that half of the incident power reaches the end plate. There is the additional higher order effect that wall losses reduce the power available for dissipation in the end plate, but this effect is negligible. The actual values for r would be slightly less. The values for r are the total of wall and end plate losses.

The calculation of the flange loss s is based on separate measurements of the loss. For instance, Yates [18] measured flange loss in WR-15 for various types of flanges and this can be extrapolated to other bands by assuming that the loss is proportional to \sqrt{f} . The thermal isolation section loss t can be calculated using the loss per unit length values for the different waveguides by simply multiplying α by the length of the section.

The parameters a , b , c , and d in eq (A1-1) are the heating effectiveness from various regions within the microcalorimeter and thermistor mount being measured. The effectiveness is calculated with respect to the heating at the thermistor bead as measured by the microcalorimeter temperature sensor. The temperature sensor is typically a thermopile or in this case a heat pump used as a sensor. The microcalorimeter is "calibrated" by applying an accurately known dc power to the bead and noting the sensor indication. When microwave power is applied, heating occurs in other regions than the bead itself. This is the reason a correction factor is needed. The value of a is 1 since the heating is caused by power in the thermistor bead, although the dc power dissipation in the bead occurs in a slightly different region than the millimeter-wave power. The bead is very small (< 0.1 mm diameter) so the difference in heating within the bead is insignificant.

The relative heating is determined using a two- (or three-) dimensional finite element thermal analysis of the specific microcalorimeter and mount. All of the millimeter wave microcalorimeters and mounts have very similar dimensions and the same geometry. Consequently, the effectiveness values will all be approximately the same.

The relative heating effectiveness through the isolation section d changes linearly from a value of approximately one at the mount flange to almost zero at the far end. As a result, one half of the heating in the isolation section is measured by the microcalorimeter sensor giving an approximate value for d of 0.5 which is representative of all the microcalorimeters.

The calculation of g using eqs (A1-1) and (A1-2) implies that all millimeter-wave losses not already discussed occur around the bead and have a relative heating effectiveness very close to one.

An example using the WR-15 microcalorimeter follows. The three frequencies shown for these calculations correspond to the ones where measurements were taken.

The loss per unit length values for WR-15 waveguide using the assumptions mentioned with eqs (A1-3) and (A1-4) are

$$\begin{aligned}\alpha &= 0.0267 \text{ dB/cm @ 50 GHz,} \\ &= 0.0189 \text{ dB/cm @ 69 GHz,} \\ &= 0.0183 \text{ dB/cm @ 75 GHz.}\end{aligned}\tag{A1-8}$$

With this information we can determine the contribution to r that is due to loss in the mount walls. The side walls are 1.25 cm long, and converting from decibels to power ratio, the fractional values for the wall loss based on the previous calculations are

$$\begin{aligned}0.0077 &\text{ @ 50 GHz (0.77 \% of incident power),} \\ 0.0055 &\text{ @ 69 GHz,} \\ 0.0053 &\text{ @ 75 GHz.}\end{aligned}\tag{A1-9}$$

The loss in the back plate of the mount is calculated using eq (A1-5) along with eqs (A1-6) and (A1-7). The fractional loss values in the end plate are

$$\begin{aligned}0.0002 &\text{ @ 50 GHz (0.02 \% of incident power),} \\ 0.0003 &\text{ @ 69 GHz,} \\ 0.0004 &\text{ @ 75 GHz.}\end{aligned}\tag{A1-10}$$

The values for r are the total of wall losses and end plate loss:

$$\begin{aligned}r &= 0.0079 \text{ @ 50 GHz,} \\ &= 0.0058 \text{ @ 69 GHz,} \\ &= 0.0058 \text{ @ 75 GHz.}\end{aligned}\tag{A1-11}$$

The calculation of the flange loss s is again based on Yates [18], who measured flange loss in WR-15 for various types of flanges. The average of a flange similar to the thermistor mount flange used in the microcalorimeter was 0.16 % (0.007 dB) of the incident power at 60 GHz. If we assume a \sqrt{f} dependence, which is appropriate for resistive skin effect losses, then the following values for s occur:

$$\begin{aligned} s &= 0.0015 \text{ @ } 50 \text{ GHz (0.15 \% of incident power),} \\ &= 0.0017 \text{ @ } 69 \text{ GHz,} \\ &= 0.0020 \text{ @ } 75 \text{ GHz.} \end{aligned} \tag{A1-12}$$

The thermal isolation section loss t is also calculated using the loss per unit length values for WR-15 waveguide. The isolation section is 0.559 cm in length so the losses are

$$\begin{aligned} t &= 0.0034 \text{ @ } 50 \text{ GHz (0.34 \% of incident power),} \\ &= 0.0024 \text{ @ } 69 \text{ GHz,} \\ &= 0.0023 \text{ @ } 75 \text{ GHz.} \end{aligned} \tag{A1-13}$$

The values for the relative heating effectiveness, a , b , c , and d , were determined using a two-dimensional analysis of the WR-10 microcalorimeter and mount. All of the millimeter-wave microcalorimeters and mounts have very similar dimensions and the same geometry so the effectiveness values are approximately equal. The two-dimensional model and three-dimensional models also agreed.

The average relative heating effectiveness in the mount walls was approximately 0.4 % less effective than heat at the bead, giving

$$b = 0.996. \tag{A1-14}$$

The average relative heating effectiveness at the mount flange was about 1 % less effective than heat at the bead, giving

$$c = 0.990. \tag{A1-15}$$

The heating effectiveness through the isolation section d changes linearly from approximately 1 at the mount flange to almost 0 at the far end. One half of the heating in the isolation section is measured by the microcalorimeter sensor giving

$$d = 0.5. \tag{A1-16}$$

The calculation of g using eqs (A1-1) and (A1-2) implies that all millimeter-wave losses not already discussed occur around the bead and have a relative heating effectiveness very close to 1. Using eq (A1-2), we have

$$\begin{aligned} q &= 0.9906 \text{ @ } 50 \text{ GHz,} \\ &= 0.9925 \text{ @ } 69 \text{ GHz,} \\ &= 0.9922 \text{ @ } 75 \text{ GHz.} \end{aligned} \tag{A1-17}$$

Then finally, by eq (A1-1)

$$\begin{aligned} g &= 1.0017 \text{ @ } 50 \text{ GHz}, \\ &= 1.0012 \text{ @ } 69 \text{ GHz}, \\ &= 1.0011 \text{ @ } 75 \text{ GHz}. \end{aligned} \tag{A1-18}$$

These values agree very well with that obtained using a flat short, the method described in section 5. At 69 GHz, the flat short measurement gives $g = 1.0014$.

The uncertainty in the above calculations is now discussed. The total differential of g in (A1-1) gives the incremental uncertainty in g . q in (A1-1) is a function of r and s . Rather than taking the partial derivatives, we will only increment each of the variables b , r , c , s , d , and t by an estimated uncertainty and note its effect on g . When the values of r or s are incremented, q must be recalculated.

The uncertainty in the loss calculations for r , s , and t is assumed to be $\pm 20\%$ in power ratio. The $\pm 20\%$ estimate is considered a conservative value. This uncertainty is due primarily to the uncertainty in the waveguide conductivity. The contribution to loss from conductivity has been experimentally verified in the WR-15 band to better than 20% of the loss for small losses (< 0.1 dB). For example, the largest loss in this analysis is 0.79% of the incident power or 0.034 dB. A 20% uncertainty in this loss would make it 0.95% , which corresponds to a loss of 0.041 dB. The 0.007 dB change is within the experimental uncertainty of a careful loss measurement.

The values of b , c , and d come from the finite element thermal analysis and are also estimated to be within $\pm 20\%$. The value for c is then 0.99 ± 0.198 which is a 2% change in relative heating effectiveness. There were seldom differences in heating effectiveness greater than 2% for different locations within the thermistor mount. Changing from two-dimensional to three-dimensional analyses or changing meshes had similar results.

The individual uncertainties in g are a weak function of frequency and are as follows:

$$\begin{aligned} &\text{uncertainty from } r = 0.0001, \text{ or } 0.01\% \\ &\text{" } s < 0.0001 \\ &\text{" } t = 0.0003 \\ &\text{" } b = 0.0015 \\ &\text{" } c = 0.0011 \\ &\text{" } d = 0.0003 \end{aligned} \tag{A1-19}$$

These uncertainties are Type B, and the plus or minus limits shown above can be considered as upper and lower limits. We assume a rectangular distribution, so the limits can be divided by $\sqrt{3}$ before combining. The combined uncertainty is the root sum of squares of the standard uncertainties and for this example is 0.0011 or 0.11% . This value agrees well with the value of 0.12% obtained for the flat short measurement.

APPENDIX 2. Determination of Incident Power Using a Directional Coupler

This appendix shows the derivation of eqs (5-38) and (5-39) from the basic scattering parameter equations for a directional coupler. The coupler ports and associated wave amplitudes are shown in Figure A2.1.

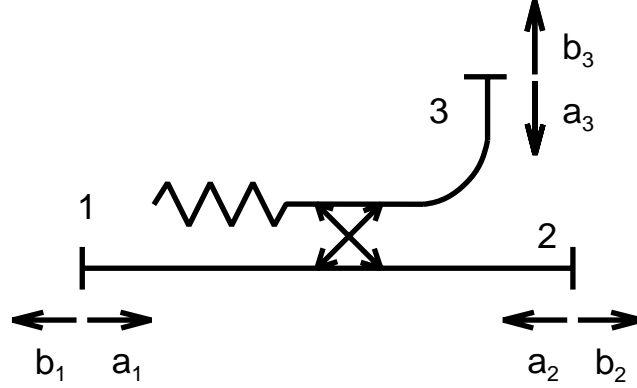


Figure A2.1 Wave amplitudes for a three-port coupler.

The scattering equations for the coupler are (see appendix 4 in [19]):

$$b_1 = S_{11} a_1 + S_{12} a_2 + S_{13} a_3, \quad (\text{A2-1})$$

$$b_2 = S_{21} a_1 + S_{22} a_2 + S_{23} a_3, \quad (\text{A2-2})$$

$$b_3 = S_{31} a_1 + S_{32} a_2 + S_{33} a_3. \quad (\text{A2-3})$$

Since the incident wave amplitude on a load attached to arm 2 is b_2 , we wish to develop an expression giving b_2 in terms of b_3 , the side arm output. Solving eq (A2-3) for a_1 and substituting into eq (A2-2) gives, after combining terms,

$$b_2 = \frac{S_{21}}{S_{31}} b_3 + \left(S_{22} - \frac{S_{21} S_{32}}{S_{31}} \right) a_2 + \left(S_{23} - \frac{S_{21} S_{33}}{S_{31}} \right) a_3. \quad (\text{A2-4})$$

The factor multiplying a_2 is the equivalent generator reflection coefficient Γ_{GE} for the coupler (appendix 4 in [18]). With a load having a reflection coefficient Γ_L attached to port 2,

$$a_2 = \Gamma_L b_2, \quad (\text{A2-5})$$

and with a detector having a reflection coefficient of Γ_D on port 3,

$$a_3 = \Gamma_D b_3. \quad (\text{A2-6})$$

Making these substitutions in eq (A2-4), combining terms and solving for b_2 gives

$$b_2 = \frac{1}{1 - \Gamma_{GE} \Gamma_L} \left(\frac{S_{21}}{S_{31}} + \left(S_{23} - \frac{S_{21} S_{33}}{S_{31}} \right) \Gamma_D \right) b_3. \quad (\text{A2-7})$$

The incident power P_I on the load connected to port 2 is given by (assuming the wave amplitudes are normalized by the characteristic impedance, see appendix 1 in [19])

$$P_I = |b_2|^2. \quad (\text{A2-8})$$

Squaring the amplitude of both sides of eq (A2-7) and substituting eq (A2-8)

$$P_I = \frac{1}{|1 - \Gamma_{GE} \Gamma_L|^2} \left| \left(\frac{S_{21}}{S_{31}} + \left(S_{23} - \frac{S_{21} S_{33}}{S_{31}} \right) \Gamma_D \right) \right|^2 |b_3|^2. \quad (\text{A2-9})$$

$|b_3|^2$ is the power incident on the port 3 detector. For this application that detector is a power sensor. In general, the power incident on a power sensor is given by the meter reading divided by the sensor calibration factor K_b (see p. 74 in [19]). Thus

$$|b_3|^2 = \frac{P_3}{K_{b3}}, \quad (\text{A2-10})$$

where P_3 is the power read by the sensor on port 3 and K_{b3} is the calibration factor for the sensor. So with eq (A2-10), plus combining all the terms that are constant for a given coupler and sensor into a single constant, eq (A2-9) can be written

$$P_I = \frac{P_3}{K_C} \frac{1}{|1 - \Gamma_{GE} \Gamma_L|^2}, \quad (\text{A2-11})$$

where

$$K_C = \frac{K_{b3}}{\left| \left(\frac{S_{21}}{S_{31}} + \left(S_{23} - \frac{S_{21} S_{33}}{S_{31}} \right) \Gamma_D \right) \right|^2}. \quad (\text{A2-12})$$

Equation (A2-11) is essentially eq (5-38) except that in eq (5-38) P_3 is replaced with P_{3L} to indicate that the power on port 3 is read with a particular load on port 2.

To determine K_C we connect a standard (calibrated) power sensor to port 2 and note the port 3 reading. Again the incident power is given by dividing the sensor reading by the sensor calibration

factor, so we have for the standard on port 2

$$P_I = \frac{P_S}{K_{bS}}. \quad (\text{A2-13})$$

In terms of measured quantities, K_{bS} is given by (also p. 74 in [19])

$$K_{bS} = \eta_S (1 - |\Gamma_S|^2), \quad (\text{A2-14})$$

where η_S is the effective efficiency of the standard and Γ_S the reflection coefficient. With eqs (A2-11), (A2-13) and (A2-14) we have then

$$\frac{P_S}{\eta_S (1 - |\Gamma_S|^2)} = \frac{P_{3S}}{K_C} \frac{1}{|1 - \Gamma_{GE} \Gamma_S|^2} \quad (\text{A2-15})$$

and solving for K_C

$$K_C = \frac{P_{3S}}{P_S} \frac{\eta_S (1 - |\Gamma_S|^2)}{|1 - \Gamma_{GE} \Gamma_S|^2}, \quad (\text{A2-16})$$

which is eq (5-39).

NIST Technical Publications

Periodical

Journal of Research of the National Institute of Standards and Technology—Reports NIST research and development in those disciplines of the physical and engineering sciences in which the Institute is active. These include physics, chemistry, engineering, mathematics, and computer sciences. Papers cover a broad range of subjects, with major emphasis on measurement methodology and the basic technology underlying standardization. Also included from time to time are survey articles on topics closely related to the Institute's technical and scientific programs. Issued six times a year.

Nonperiodicals

Monographs—Major contributions to the technical literature on various subjects related to the Institute's scientific and technical activities.

Handbooks—Recommended codes of engineering and industrial practice (including safety codes) developed in cooperation with interested industries, professional organizations, and regulatory bodies.

Special Publications—Include proceedings of conferences sponsored by NIST, NIST annual reports, and other special publications appropriate to this grouping such as wall charts, pocket cards, and bibliographies.

Applied Mathematics Series—Mathematical tables, manuals, and studies of special interest to physicists, engineers, chemists, biologists, mathematicians, computer programmers, and others engaged in scientific and technical work.

National Standard Reference Data Series—Provides quantitative data on the physical and chemical properties of materials, compiled from the world's literature and critically evaluated. Developed under a worldwide program coordinated by NIST under the authority of the National Standard Data Act (Public Law 90-396). NOTE: The Journal of Physical and Chemical Reference Data (JPCRD) is published bi-monthly for NIST by the American Chemical Society (ACS) and the American Institute of Physics (AIP). Subscriptions, reprints, and supplements are available from ACS, 1155 Sixteenth St., NW, Washington, DC 20056.

Building Science Series—Disseminates technical information developed at the Institute on building materials, components, systems, and whole structures. The series presents research results, test methods, and performance criteria related to the structural and environmental functions and the durability and safety characteristics of building elements and systems.

Technical Notes—Studies or reports which are complete in themselves but restrictive in their treatment of a subject. Analogous to monographs but not so comprehensive in scope or definitive in treatment of the subject area. Often serve as a vehicle for final reports of work performed at NIST under the sponsorship of other government agencies.

Voluntary Product Standards—Developed under procedures published by the Department of Commerce in Part 10, Title 15, of the Code of Federal Regulations. The standards establish nationally recognized requirements for products, and provide all concerned interests with a basis for common understanding of the characteristics of the products. NIST administers this program in support of the efforts of private-sector standardizing organizations.

Consumer Information Series—Practical information, based on NIST research and experience, covering areas of interest to the consumer. Easily understandable language and illustrations provide useful background knowledge for shopping in today's technological marketplace.

Order the above NIST publications from: Superintendent of Documents, Government Printing Office, Washington, DC 20402.

Order the following NIST publications—FIPS and NISTIRs—from the National Technical Information Service, Springfield, VA 22161.

Federal Information Processing Standards Publications (FIPS PUB)—Publications in this series collectively constitute the Federal Information Processing Standards Register. The Register serves as the official source of information in the Federal Government regarding standards issued by NIST pursuant to the Federal Property and Administrative Services Act of 1949 as amended, Public Law 89-306 (79 Stat. 1127), and as implemented by Executive Order 11717 (38 FR 12315, dated May 11, 1973) and Part 6 of Title 15 CFR (Code of Federal Regulations).

NIST Interagency Reports (NISTIR)—A special series of interim or final reports on work performed by NIST for outside sponsors (both government and non-government). In general, initial distribution is handled by the sponsor; public distribution is by the National Technical Information Service, Springfield, VA 22161, in paper copy or microfiche form.